ELSEVIER

Nuclear Instruments and Methods in Physics Research A 370 (1996) 579-596

NUCLEAR
INSTRUMENTS
& METHODS
IN PHYSICS
RESEARCH
Section A

Light concentrators for the Sudbury Neutrino Observatory

G. Doucas[a], S. Gil[b,1], N.A. Jelley[a,*], L. McGarry[b], M.E. Moorhead[a], N.W. Tanner[a], C.E. Waltham[b]

[a] *Nuclear Physics Laboratory, Oxford University, Keble Road, Oxford, England OX1 3RH, UK*
[b] *Physics Department, University of British Columbia, Vancouver B.C., Canada V6T 1Z1*

Received 17 July 1995

Abstract

There is an important and growing class of elementary particle detectors which are characterized by a large sensitive volume (thousands of tonnes), very low radioactive backgrounds, and rely on the emission of light for particle detection. Water Cherenkov detectors come into this category; they have a large mass of water as the sensitive medium. Particles are detected when they interact with the water and produce Cherenkov light, so detection efficiency relies on having a huge light sensitive area at the periphery of the detector. The most cost-effective way of achieving this is by placing light concentrators on large photomultiplier tubes (PMTs). This paper describes the work carried out on light concentrators for the PMTs in the Sudbury Neutrino Observatory, a 1000 tonne heavy water Cherenkov detector. We discuss the advantages of using light concentrators, summarize the optical theory of non-imaging light concentration, and describe in detail the development and manufacture of the concentrators themselves.

1. Introduction

The light concentrators we consider are devices which take light incident on an entrance aperture over a given angular range, and direct it by reflection from a curved surface onto a smaller exit aperture. There is thus a gain in collection efficiency with a corresponding reduction in angular coverage in accordance with phase space volume conservation. The Winston cones on the end of light guides are an example of light concentrators familiar to particle physics. The concentrators we describe in this paper are a development of the Winston cone for use on spherical PMTs.

1.1. Large water Cherenkov detectors

When elementary charged particles pass through a medium at a speed which is faster than the local speed of light, they radiate "Cherenkov light" [1]. These photons have a $1/\lambda^2$ wavelength distribution, but those with $\lambda < 300$ nm are usually absorbed in detector components, so the useful light is predominantly in the blue and near UV. In water the average speed of light is 0.75 times that in a vacuum, and so a body of water, instrumented with light sensors, forms an effective detector for any charged particle travelling faster than this. Because water is cheap and transparent, it lends itself to non-accelerator particle physics experiments where low event rates require huge detectors, particularly for the detection of relativistic electrons from neutrino scattering and proton decay [2,3].

A typical size for this class of detector is a few thousand tonnes, i.e. of order 10 m radius. This requires light detectors which cover a fair fraction of the surface area of the water tank - hundreds of square metres - particularly when looking for low energy events which produce few Cherenkov photons. Two such detectors have been built on a 1000 tonne scale - IMB in Ohio [4] and Kamiokande [5] in Japan. Both were originally designed to search for proton decay, both attained fame by detecting neutrinos from Supernova SN1987A, and now Kamiokande has been modified to lower its energy threshold for the observation of solar neutrinos. Two additional Cherenkov detectors are being built on a scale as large or larger: the Sudbury Neutrino Observatory, with which we are presently concerned, and SuperKamiokande [6], a 50000 tonne light water Cherenkov detector.

At present the only serious option in light detection is an array of photomultiplier tubes (PMTs). It is now possible to obtain PMTs which have relatively large sensitive areas (of the order 1000 cm^2 each) for relatively low cost (several hundred dollars), with good timing (a few ns) and good quantum efficiency (~20%). Moreover, the effective area of a PMT can be significantly improved by using light con-

---

[*] Corresponding author. Tel. +44 1865 273380, fax +44 1865 273418, e-mail n.jelley@physics.oxford.ac.uk.

[1] Present address: TANDAR, Departamento de Física, Comisión Nacional de Energía Atómica, Av. del Libertador 8250, 1429 Buenos Aires, Argentina.

0168-9002/96/$15.00
SSDI 0168-9002(95)00840-3

centrators, and this approach is particularly useful in spherically symmetric detectors such as the Sudbury Neutrino Observatory.

1.1.1. The Sudbury Neutrino Observatory

The Sudbury Neutrino Observatory (SNO) is a heavy water Cherenkov detector [2] that will be located in an INCO nickel mine near Sudbury, Ontario, Canada. It is being built in a cylindrical cavern at a depth of 2070 m underground to provide adequate shielding from atmospheric cosmic radiation. The cavern has a diameter of 22 m and a height of 32 m. Inside there will be constructed a spherical acrylic vessel, with a diameter of 12 m, containing 1000 tonnes of heavy water (D_2O). Surrounding the D_2O will be 7000 tonnes of ultra-pure light water (H_2O) for mechanical support and as a shield from background radiations from the surrounding rock. Around the acrylic vessel and suspended in the light water will be a geodesic frame holding 9500 PMTs and light concentrators (see Fig. 1).

Its primary purpose is to resolve the longstanding discrepancy between the solar neutrino capture rate in ^{37}Cl predicted by the Standard Solar Model (SSM) and the rate measured by the chlorine-based experiment in the Homestake Gold Mine. The measured rate averaged over 1970-1988 is less than half of the predicted rate. In 1989 a discrepancy was also reported by the Kamiokande II water Cherenkov radiation experiment, which observed a neutrino flux about a half that predicted by the SSM. Recently the results of the Gallium experiments [7,8] which are sensitive to the low energy neutrinos from the pp cycle show that the flux of low energy neutrinos is also lower than that calculated by the SSM.

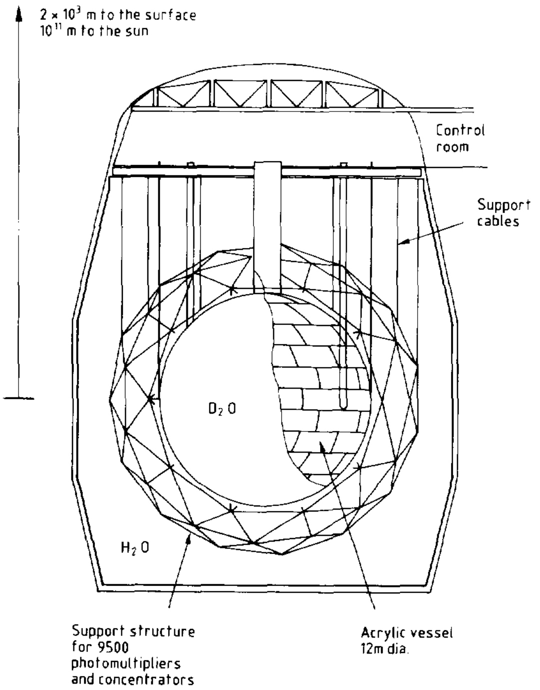

Fig. 1. Schematic Representation of the SNO Detector. The PMTs and concentrators are mounted on a geodesic frame 8.5 m in radius.

Solutions to the "solar neutrino problem" have been put forward which invoke either non-standard solar models or new particle physics. The ^{37}Cl and Kamiokande experiments are primarily sensitive to the high energy ^{8}B solar neutrinos. Numerous non-standard models which reduce the core temperature have been proposed but none have been able to reproduce the observed ^{8}B flux and all other observed features of the sun, while still being consistent with our knowledge of stellar evolution [9].

The most plausible explanation involving new particle physics is the resonant enhancement of neutrino oscillations by the matter in the sun (the MSW effect [10]). In this explanation the majority of the ^{8}B neutrinos undergo conversion in their passage through the sun into muon or tau neutrinos, to which existing experiments have little (Kamiokande) or no (^{37}Cl, ^{71}Ga) sensitivity.

The major advantage of the SNO detector is that the use of D_2O as a detecting medium enables not only the flux and energy spectrum of electron neutrinos but also the total flux of all neutrino types above an energy of 2.2 MeV to be measured. With these two measurements it will be possible to show clearly, independent of solar models, whether neutrino oscillations are occurring, and also to test solar models by determining the production rate of high-energy electron neutrinos in the solar core [2].

The primary detection reactions are:

$$\text{(I)}\ \nu_e + \mathrm{d} \longrightarrow \mathrm{p} + \mathrm{p} + \mathrm{e}^-,$$
$$\text{(II)}\ \nu_x + \mathrm{e}^- \longrightarrow \nu_x + \mathrm{e}^-,\ \text{where } x = \mathrm{e}, \mu, \tau,$$
$$\text{(III)}\ \nu_x + \mathrm{d} \longrightarrow \mathrm{p} + \mathrm{n} + \nu_x.$$

Reaction (I) is detected by the Cherenkov light from the relativistic electron. It is currently expected that the electron energy detection threshold will be ~5 MeV; at lower energies there is a steeply rising background due to radioactivity. The Q-value for this reaction is -1.44 MeV. Thus, only electron neutrinos with energy greater than ~6.5 MeV will be detected.

Reaction (II) is also detected by the Cherenkov light from the scattered electron. Its rate is about 1/9 of reaction (I), and it can be distinguished from reaction (I) by the electron's angular distribution with respect to the position of the sun (strongly forward peaked).

Reaction (III) will be detected as a result of the neutron being captured radiatively on a ^{35}Cl atom, producing a total of 8.6 MeV in γ-rays. These γ-rays will shower in the water and produce Cherenkov light. The ^{35}Cl will be in the form of an aqueous solution of $MgCl_2$ in the heavy water.

---

[2] We assume here that the neutrinos oscillate into detectable left-handed neutrinos and not into "sterile" right-handed ones.

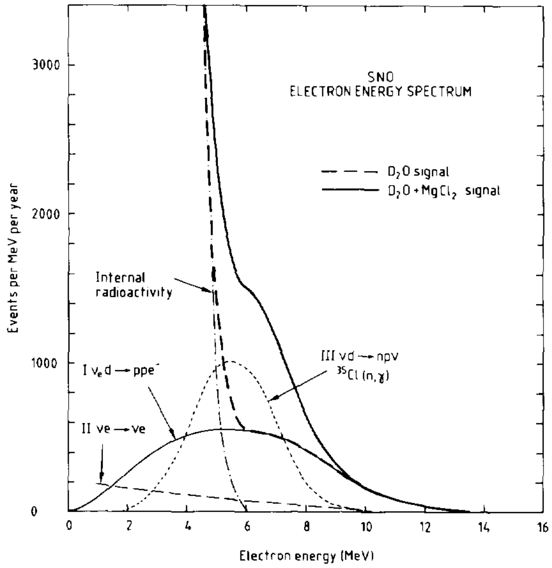

Fig. 2. A simulation of the number of electron events expected to be observed in SNO after one year of running. The signals from reactions (I), (II) and (III) are shown; in practice these will have to be untangled from each other by the use of data taken with and without ^{35}Cl, by the use of angular distributions and by the use of ^{3}He proportional counters. For reactions (II) and (III) the total flux of neutrinos is assumed to be given by the SSM, while for reaction (I) the flux is assumed to be one third of the SSM.

A simulation of the number of neutrino events expected to be observed in the SNO detector after one year of running is shown in Fig. 2; the contributions from reactions (I), (II) and (III) are indicated together with the background caused by internal radioactivity.

A very important experimental requirement for the accurate determination of the neutral current neutrino induced reaction (III) is that materials in the detector, and in particular the heavy water, must have very little thorium and uranium. High energy γ-rays at the bottom of the thorium and uranium chains can dissociate deuterium, and this process is indistinguishable from reaction (III).

With $MgCl_2$ added to the D_2O, Cherenkov photons originating from all three reactions will be observed; the angular distribution of those from reaction (III) is different from that from either reactions (I) or (II). These differences, together with data taken with no $MgCl_2$ added to the D_2O, will be used to determine the rates for all three reactions. In addition, it is planned to use very low background ^{3}He proportional counters in the D_2O to detect the neutrons generated by reaction (III). This will provide a way of detecting the neutral current events from reaction (III) separately and concurrently with the charged current events from reaction (I) and the charged and neutral current events from reaction (II).

By comparing the observed rates for these reactions, particularly (I) and (III), which have high rates (each of the order 10 per day, which is large for neutrino astrophysics), we will be able to tell if the ν_e leaving the sun arrive at the earth as neutrinos of other flavours. The successful operation of the detector relies on the efficient detection of Cherenkov photons.

1.1.2. The effects of using light concentrators

It is expected that SNO will be able to identify electron tracks only if their energy is greater than about 5 MeV. Below 5 MeV there is a large background caused by photons arising from radioactive decays in the detector materials and the water. Now the low energy part of the solar neutrino spectrum is very sensitive to some possible oscillation effects and it is critical that the neutrino detection threshold be as low as possible [2,3]. The use of light concentrators on the PMTs will increase our photon detection efficiency by 75%. There are two consequences of this, both of which will reduce this background:

- The increase in the number of photons detected from a given electron track helps to define that track better, in energy and geometry, by reducing statistical uncertainties.

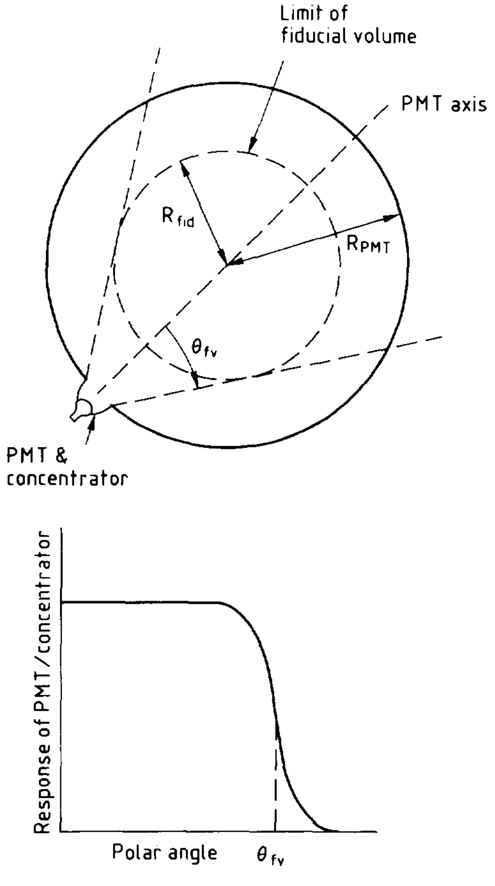

Fig. 3. The geometry of SNO which determines the characteristics of the concentrator and the angular response of a practical concentrator.

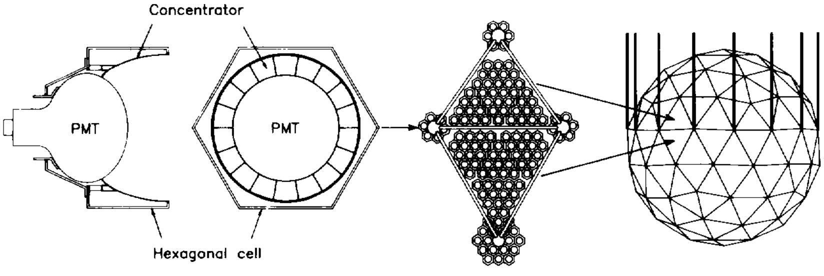

Fig. 4. Sketchs of PMT and concentrator in hexagonal cell mounting and of the make-up of the geodesic sphere from panels of hexagonal cells. (The design of the hexagonal cell and geodesic sphere was carried out at the Lawrence Berkeley Laboratory.)

A better defined track can more easily be distinguished from low energy radioactivity events, most of which originate in detector materials other than the D_2O, and can be removed by energy, fiducial cuts, or a combination of both.

- The PMTs themselves are relatively high in radioactive materials (~25 ppb by weight each of Th and U), despite being made of the cleanest glass available, so it is desirable that each PMT is shielded optically from its neighbours to reduce the chance of accidental coincidences. The light concentrators fulfil this purpose.

The optical geometry which determines the design of the concentrators is shown in Fig. 3. An ideal PMT and concentrator combination would only be sensitive to light generated up to a certain critical angle θ_{fv} away from the PMT axis. The fiducial volume defined by this angle has a radius R_{fid}; in SNO this is set at 7 m, slightly larger than the 6 m radius of the D_2O volume to ensure no loss of sensitivity near the edge and to provide some H_2O coverage, and also to see the background associated with the wall of the acrylic vessel. In SNO each PMT and concentrator is held in an ABS plastic hexagonal cell, and several of these cells are bolted together to form flat panels. These panels are joined together to make a geodesic sphere with a mean radius of R_{PMT} ~8.5 m. A schematic diagram of these components is shown in Fig. 4.

2. Optical theory

The optics of nonimaging light concentration has been well developed over the past twenty five years by Welford and Winston [11] and others. Two of the most fruitful applications of this work have been in solar energy generation and in elementary particle physics detectors. In both cases it is important to maximize the number of photons detected, so the use of concentrators is particularly appropriate. With a nonimaging concentrator, then, for a wide range of incident angles within the acceptance angle, such devices can approach the theoretical limit of light concentration.

2.1. Theory of nonimaging concentrators

The tangent-ray principle of Welford and Winston gives a prescription for designing a concentrator in two dimensions. This tangent-ray principle states that the concentrator should be designed such that, after the first reflection, the rays incident upon the entry aperture at an extreme angle θ_i strike the absorber tangentially (see Fig. 5). With such a design, if the incident angle is less than θ_i, the ray is reflected into the absorber, and if the incident angle is greater than θ_i, the ray misses the absorber and is reflected out of the concentrator. In two dimensions, θ_i is the cut-off angle.

In our case the "absorber" is the photocathode of a PMT, nearly spherical and with a polar extent θ_c. A three-dimensional concentrator is generated by rotating the two-dimensional profile around the optic axis. It is not possible to preserve the perfect 2D performance in three dimensions; there are problems with skew rays which cause the acceptance to fall off gradually at angles $< \theta_i$. These problems are associated with the difference between the phase space limits on angular acceptance in 3D and in 2D and an even more stringent limitation imposed on the 3D angular acceptance by the conservation of angular momentum. These effects are summarized for the case of a spherical photo-

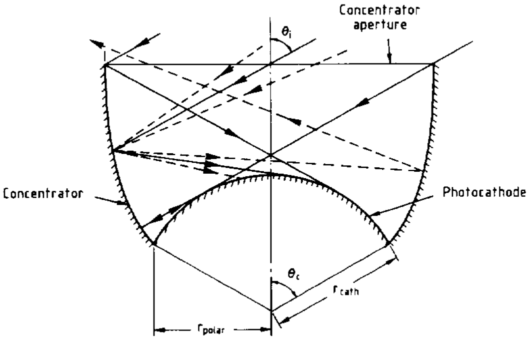

Fig. 5. A exact 2D concentrator constructed according to the tangent-ray principle. The solid rays incident at the entrance aperture at the limiting polar angle θ_i are reflected to be tangential to the photocathode.

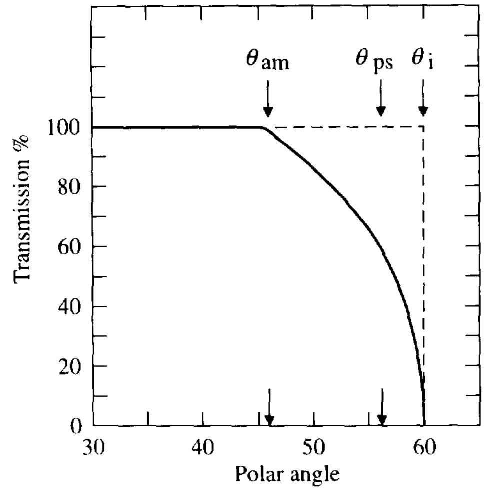

Fig. 6. Calculated transmission curve for a concentrator designed for $\theta_i = 60°$ and $\theta_c = 60°$, for which $\theta_{am} = 45.7°$ and $\theta_{ps} = 55.8°$.

cathode in the following equations. (For a full derivation the reader is directed to Moorhead and Tanner [12,13], where the more general case of a non-spherical photocathode is also discussed.)

The relation between the phase space cut-off angles θ_{ps} (in 3D) and θ_i (in 2D) for a spherical absorber is given by

$$\sin\theta_{ps} = \frac{\sin(\theta_c/2)}{\theta_c/2}\sin\theta_i . \tag{1}$$

Skew invariance, or the conservation of the axial component of angular momentum, causes the transmission of a concentrator to fall off when $\theta > \theta_{am}$ where

$$\sin\theta_{am} = \frac{\sin\theta_c}{\theta_c}\sin\theta_i , \tag{2}$$

so $\theta_{am} < \theta_{ps} < \theta_i$. For spherical photocathodes with $\theta_c > 30°$ the start of the fall off in transmission is determined by θ_{am}. This is illustrated in Fig. 6 which shows the calculated transmission curve for a concentrator designed for $\theta_i = 60°$ and $\theta_c = 60°$, for which $\theta_{am} = 45.7°$ and $\theta_{ps} = 55.8°$.

The geometrical concentration factor, C_{geo}, which is the ratio of the area of the entrance aperture of the concentrator, A_{conc}, to that of the curved photocathode, A_{cath} is given by:

$$C_{geo} = \frac{A_{conc}}{A_{cath}} = \frac{1}{\sin^2\theta_{ps}} , \tag{3}$$

where $A_{cath} = 2\pi r_{cath}^2(1-\cos\theta_c)$. Now the increase in light collection efficiency equals the projected concentration factor C_{proj}, which is the ratio of A_{conc} to the projected area of the photocathode A_{proj} (i.e. the area of the exit aperture of the concentrator):

$$C_{proj} = \frac{A_{conc}}{A_{proj}} = \frac{1}{\cos^2\frac{\theta_c}{2}\sin^2\theta_{ps}} = \frac{A_{cath}}{A_{proj}\sin^2\theta_{ps}} . \tag{4}$$

2.2. Application to spherical detectors

The concentrator we shall discuss was designed with the particular geometry and PMT (Hamamatsu R1408) of SNO in mind, i.e. an effective photocathode polar extent of $\theta_c = 54.5°$, corresponding to a polar radius $r_{polar} = 98$ mm (see Fig. 5) and acceptance angle $\theta_{ps} = 56.4°$. The ideal concentration factor values are thus $C_{geo} = 1.441$ and $C_{proj} = 1.824$. These assume no divergence of light at the front aperture of the concentrator. In SNO (see Fig. 3) the choice of which angle θ_i , θ_{am} or θ_{ps} to match to the edge of the fiducial volume is $\theta_{ps} = \theta_{fv}$. For this choice then the divergence, θ_{div}, of light is: $\theta_{div} = l_{cath}/R_{fid} = 1°$, where $A_{cath} = \frac{\pi}{4} l_{cath}^2$. So the assumption of no divergence is a good one.

There is a special result that occurs when both the detector fiducial volume and the array of PMTs are spherically symmetric, as in SNO. The probability of detecting light from anywhere inside a spherical fiducial volume (radius R_{fid}) is proportional to the fractional coverage, f, provided by N_{pmt} PMTs and concentrators placed on a sphere, radius R_{pmt} ($> R_{fid}$).

$$f = \frac{A_{conc}N_{pmt}}{4\pi R_{pmt}^2} . \tag{5}$$

Note, however, that $A_{conc} = A_{cath}/\sin^2\theta_{ps}$, and $\sin\theta_{ps} = R_{fid}/R_{pmt}$, so that:

$$f = \frac{A_{cath}N_{pmt}}{4\pi R_{fid}^2} . \tag{6}$$

Now f is independent of R_{pmt} for a fixed number of PMTs, and R_{pmt} can be increased without losing photons, providing the concentrators are modified accordingly and absorption in the water is not important. The coverage allowed by the use of ideal concentrators is the same as that obtained by placing the PMTs at the edge of the fiducial volume and flattening out the photocathodes to conform with the boundary!

The radial efficiency of a spherical array of PMT's is not R_{pmt} times the polar angular response of a single PMT, as light for polar angles less than θ_{fv} ($< \theta_{ps}$ in SNO) can arise from points both inside and outside the fiducial volume (see Fig. 3), with the result that the radial efficiency falls off less markedly than the angular response of a single PMT. In SNO the radius R_{pmt} was chosen to optimize the shielding of the heavy water from the radioactivity of the PMTs, and of the PMTs from the radioactivity of the wall of the cavern. The size of the cavern was entirely constrained by mine engineering limitations.

3. Practical design of non-imaging concentrators

3.1. Photomultiplier tube considerations

Real photocathodes have a slightly non-uniform angular response, which has been measured and modelled optically [13-16]. Shown in Fig. 7 [13], for a Hamamatsu R1408

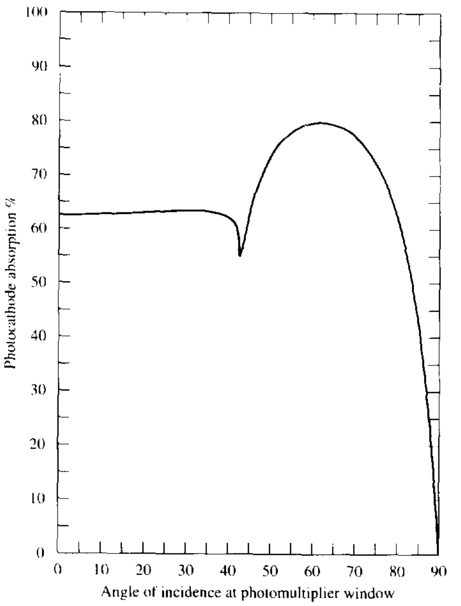

Fig. 7. The predicted angular dependence of the absorption of the bialkali photocathode for a Hamamatsu R1408 8 in. PMT in water [13]. The absorption is proportional to the PMT efficiency [14]. Plotted is the percentage of incident intensity which is absorbed by the photocathode, where for 0° to 40° an allowance of 5% has been included as an estimate of the effect of internal reflections of light transmitted through the photocathode.

8 in. PMT immersed in water, is the photocathode absorption, which has been shown to be proportional to the PMT efficiency [14]. The efficiency drops to zero at grazing incidence when all the light is reflected off the water-glass interface, and is roughly half its average value at the angle of incidence $\theta_r = 85°$. This reduces the cut-off angle θ_{ps} slightly. The relationship between concentration factor C_{geo} and these angles is given by phase-space considerations:

$$C_{geo} = \frac{\sin^2\theta_r}{\sin^2\theta_{ps}}. \tag{7}$$

This is the general case of that given above where θ_r is 90° for a perfect absorber. Now C_{geo} is determined by the geometry of the concentrator, so a change in θ_r will reduce θ_{ps}. Using the numbers given above, if θ_r is 85°, then θ_{ps} changes from 56.4° to 56.1°, a reduction of only 0.3°.

Besides the slight non-uniform angular response, real photocathodes show a fall-off in efficiency for light falling near the edge of the photocathode. For the PMT (Hamamatsu R1408) used in SNO, a concentrator with a slightly larger polar radius r_{polar} than 98 mm, but with the same θ_{ps}, would increase the average concentration factor, as θ_c would be larger. However, the concentration factor would not be significantly increased for light incident at small polar angles, as this is funneled onto the edge of the photocathode where the efficiency is low. The choice of $r_{polar} = 98$ mm was a compromise between *maximum* and *uniform* concentration.

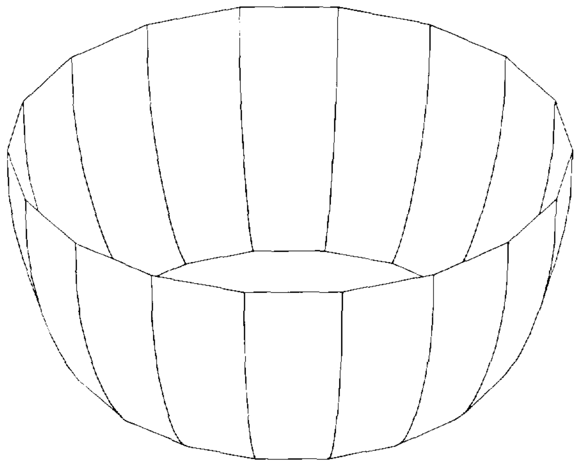

Fig. 8. A polygonal approximation to the shape of a concentrator.

3.2. Polygonal symmetry

The shape of an ideal concentrator may be approximated by a polygonal shape (see Fig. 8). This allowed us to consider reflective materials which were only available as flat sheets, as these could be curved (in one direction) and joined together into a polygonal shape.

How the performance of polygonal specular concentrators differs from the cylindrically symmetric case can be expressed in the sharpness of the drop-off near the cut-off angle. For a polygonal cross-section, θ_{ps} will vary somewhat with azimuthal angle. A measure of sharpness is the angular spread between the points where the concentrator response is 90% and 10% of its maximum; Table 1 shows how this quantity varies with the number of faces of the polygon [17].

3.3. Truncation

Ray-tracing simulations showed that the ideal concentrator determined by the prescription given above could be truncated in length by a quarter with a reduction in concentration factor of only 2%, and the appearance of a small tail in the large-angle acceptance (Fig. 9a). As can be seen (Fig. 9b), the difference between a truncated figure-of-revolution and a truncated 18-sided polygonal concentrator is very small. In fact in the longer concentrator there are more reflections and consequently more opportunities for absorption. A shorter concentrator is cheaper, lighter and easier to manufacture.

Table 1
Performance of polygonal concentrators

Number of faces	Angular spread: 90-10% [deg]
6	14.0
12	10.3
18	9.2
∞	9.0

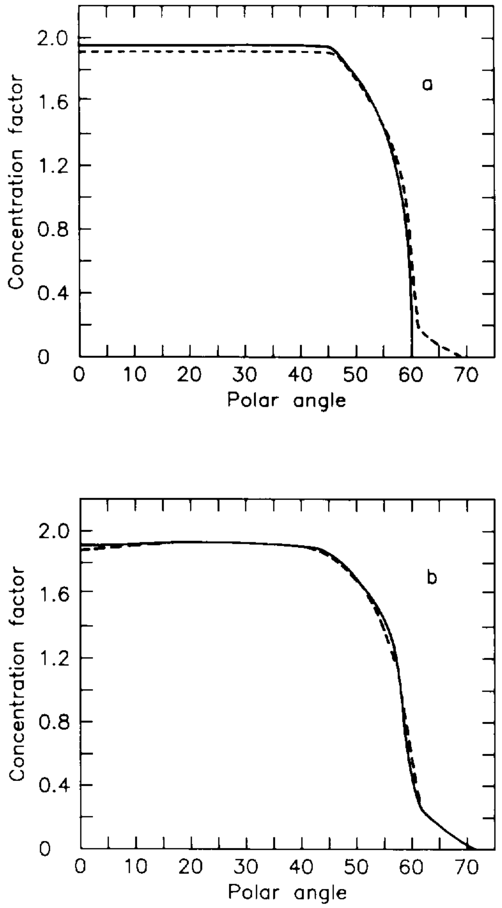

Fig. 9. A comparison of the concentration factors for (a) a full-length (solid line) and a truncated figure-of-revolution concentrator in which the entrance aperture area has been decreased by 2%; (b) a truncated figure-of-revolution (solid line) and a truncated 18-sided polygonal concentrator. The simulation assumes ideal reflective surfaces and ideal photocathodes.

The final shape of the SNO concentrator was chosen to optimize the transmission of off-axis or skew rays with a skew parameter $h_{\rm rel} = 0.6$ [12,13]. While very similar in performance to that obtained by rotating the 2D profile about the optic axis for which $h_{\rm rel} = 0.0$, it has the advantage that the axial length of the concentrator is slightly reduced (to 142 mm from 154 mm). This length was then truncated by 24% to 108 mm.

3.4. Dimensional tolerances

Any inaccuracies in construction or flexing inside the PMT/concentrator support frame will have a detrimental effect on the optical performance of the concentrator. The subject of tolerances divides into three areas: imperfections in manufacture (particularly conformity of the dielectric-coated aluminium strips to the holder), misalignment of whole concentrators, and flexing of concentrators.

The effect of imperfectly curved strips in a polygonal concentrator is small as the concentrator is a non-imaging device. For the SNO concentrator described below in Section 4, the deviation from the correct curvature is expected to be less than ~ 0.4 mm. The effect of such an alteration in curvature is too small to be seen easily so the change in response for a reduction in curvature corresponding to a maximum deviation of about 3.5 mm from the correct curvature some 50 mm from the face of the PMT is shown in Fig. 10. Even this much larger deviation would only result in a decrease of the angle $\theta_{\rm ps}$ of about 2°, equivalent to a 6.5% reduction in the volume coverage.

The arrangement of the hexagonal cells into flat panels means that the PMTs plus concentrators are not all pointing at the centre of the acrylic vessel but are all aligned within 3°. As the drop-off in efficiency is spread over 9° about $\theta_{\rm ps}$, then this degree of misalignment has no significant effect on the performance of the detector. This is borne out by simulations which have shown that for a random alignment of the concentrators between 0° and θ off the centre, then θ has to be greater than 7° before the light collection from the fiducial volume is significantly affected [18].

Sufficient flexing of one of the panels holding the PMT and concentrator could cause the front aperture of the concentrator to distort into an ellipse of major axis A and minor axis B. To first order the aperture area is conserved as $A \times B = R^2$, where R is the radius of the entrance aperture; a 1% distortion will produce a second order effect of about 0.01%. More serious is that the distorted concentrator is no longer symmetric about the optic axis and depends on ϕ, the angle from the major axis of the entrance aperture ellipse. The photons incident at the concentrator aperture with $\phi \approx 0°$ or 180° will be concentrated onto the PMT with an average cut-off angle θ_A, and those with $\phi \approx 90°$ or 270° will be concentrated with a cut-off angle θ_B, where conservation of phase space gives the following expression to first order:

$$A \sin\theta_A = B \sin\theta_B = R \sin\theta_{\rm ps}\,.$$

The diameter of the concentrator is 273 mm, so a distortion of ±1.5 mm in the diameter corresponds to a 1° variation in cut-off angle. As the drop-off in efficiency is spread over 9° about $\theta_{\rm ps}$, then such a distortion to the concentrators will have a negligible ($\ll 1\%$) effect.

3.5. Choice of materials

The requirements for the reflecting material can be divided into the following areas: reflectance, durability and leaching characteristics in ultra-pure water, radioactivity, cost and ready availability.

3.5.1. Reflectance

The desire to detect as many photons as possible dictated that the reflectance of the concentrators be as high as possible for blue and near UV photons incident over a large range

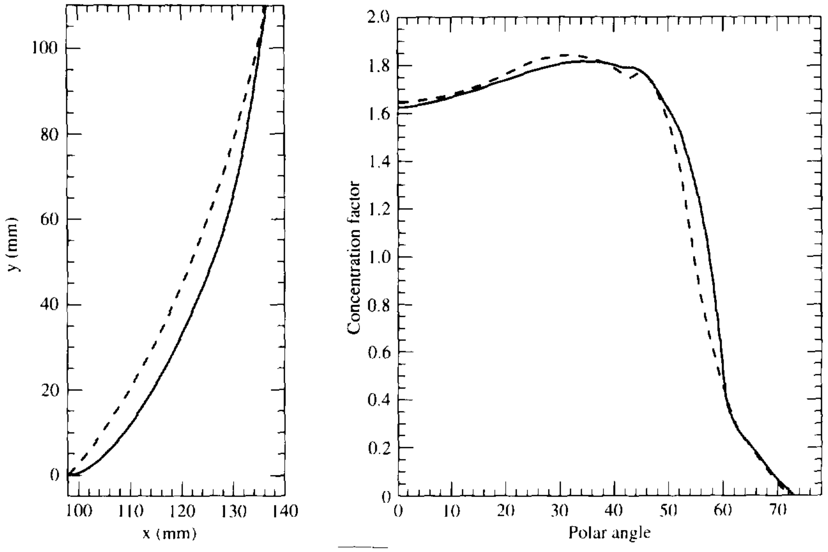

Fig. 10. The change in response of the SNO concentrator for a reduction in curvature of the strips corresponding to a maximum deviation of about 3.5 mm from the correct curvature some 50 mm from the face of the PMT. The designed shape and calculated response in water are shown by the solid lines, the changed shape and response by the dashed lines. The angle θ_{ps} is reduced by about 2°, equivalent to a 6.5% reduction in the volume coverage.

of angles. The geometrical construction described above assumed that this reflectance is specular. While this is possible to achieve with actual materials to a very good approximation, the magnitude of the reflectance will generally be noticeably less than 100%. However, the decrease in concentration factor is significantly less than the corresponding decrease in reflectance. This is because up to half of the concentrated light at a given angle θ is *directly* incident on the photocathode without being reflected off the concentrator. At large θ the proportion of light decreases while for small θ much of the light is multiply reflected, both effects decreasing the concentration factor slightly giving an approximately constant reduction factor R compared with the response with 100% reflectance. The values of R_x, where x is the percentage reflectance, are: $R_{90} = 0.95$, $R_{80} = 0.89$ and $R_{70} = 0.84$.

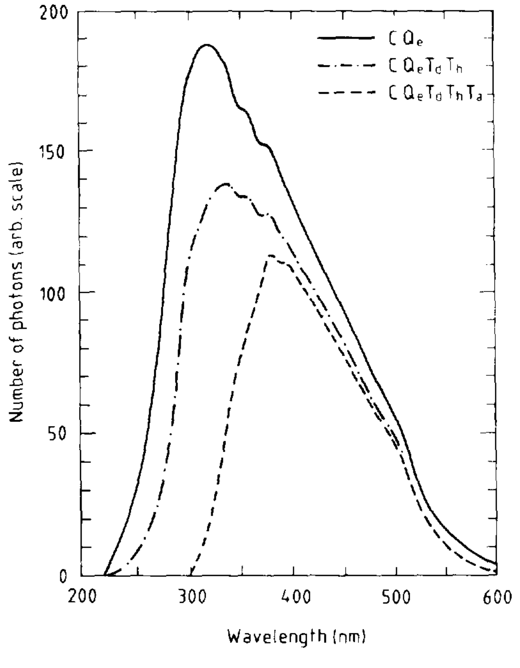

Fig. 11. The effective wavelength spectrum for the detected Cherenkov light from events inside the D_2O. The symbol C is the $1/\lambda^2$ spectrum of Cherenkov radiation, Q_e is the measured quantum efficiency of an R1408 PMT, and T_d, T_h and T_a are the average transmissions of the D_2O, H_2O and acrylic vessel.

The spectral distribution of incident photons is shown in Fig. 11, along with the spectral response of the PMTs. The distribution of incidence angles to the normal of the concentrator reflective surface is shown in Fig. 12 for photons generated uniformly throughout the fiducial volume (D_2O plus 1 m of H_2O) of SNO. Any optimization of reflectance had to be done with reference to these two distributions.

The requirement of high reflectance in the near UV narrowed the search very early to different forms of aluminium (with one exception), which is the only common metal which remains highly reflective in this region. Reflectance measurements were made with spectrophotometers in various manners as discussed below and in Ref. [19]

3.5.2. *Durability in water*

The SNO detector is planned to operate for a least five years. It was decided that any candidate reflector material

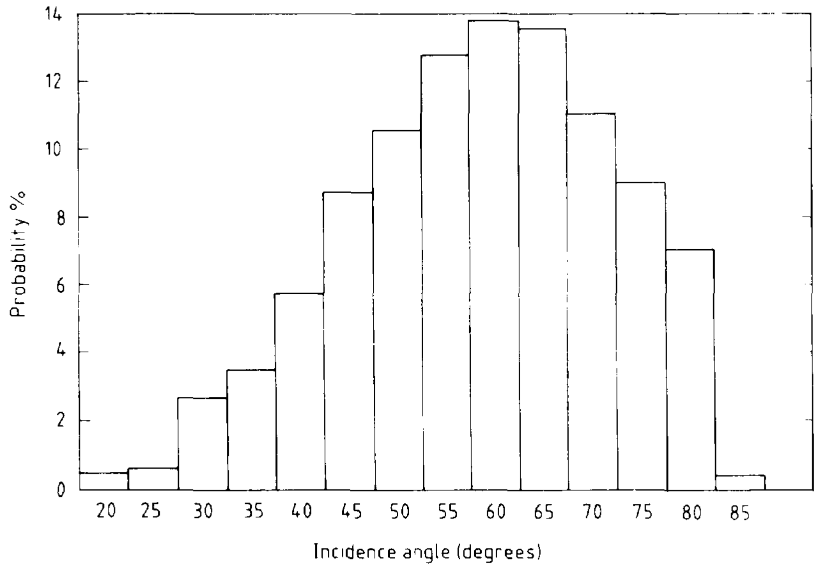

Fig. 12. The distribution of incidence angles to the normal of the concentrator reflective surface for photons generated uniformly throughout the fiducial volume (D_2O plus 1 m of H_2O) of SNO.

had to survive for an equivalent of at least ten years in deionized water at 8°C. Survivability was defined in terms of the drop in optical performance after that period of aging. Durability was assessed by immersion in hot deionized water for periods of time. It was assumed that any physical or chemical aging process would be governed by thermodynamic considerations and the rate would increase by at least a factor of two for every 10°C rise in temperature. Hence, a period of ten days immersion at 95°C was assumed to be the equivalent of ten years immersion at 8°C. This test was used to assess candidate materials in the early stages of the selection process (although it was too high a temperature for some possible protective materials such as wax). This exponential behaviour of corrosion rate with temperature is supported by an extensive body of empirical evidence. However, the precise value of the exponential factor is not known *a priori* and does vary slightly according to the exact chemical process of corrosion. It is the poor knowledge of this exponential factor (and the possibilities of phase changes in the materials) which underlies the difficulty of extrapolating the results of accelerated aging tests over large temperature ranges. Tests at lower temperatures were also carried out, but these necessarily took much longer.

Of general concern in SNO is the leaching of materials into the water which may increase the radioactivity of the water and thereby increase the background. Leaching also loads the water purification system and provides potential trace nutrients for biological activity. Biological activity in the water can have a detrimental effect on light transmission [20]. In practice, leaching was not a problem for the optical surfaces themselves, which would not survive if any significant leaching occurred.

3.5.3. *Radioactivity*

The response of SNO is limited at low energy by radioactive backgrounds, some of which originate in the PMT glass. Thus it was required that the additional radioactivity of the concentrators did not raise this threshold significantly and defeat their original purpose.

3.5.4. *Cost and availability*

The cost of each PMT and associated electronics for SNO is about $C1000. Given that the concentrators will increase the effective area of a PMT by 75%, it was desirable that the unit cost of a concentrator be much less than $C500.

3.6. *Reflective materials considered*

The only common specular material with high reflectance in the wavelength range of Cherenkov light in SNO (300-600 nm) is aluminium. Indeed, for use in vacuum, the simplest reflective material to use would be bare, evaporated aluminium. However, this being readily oxidised in water, at least for the layer thicknesses and timescales under consideration, it was necessary to find a means of protecting it without compromising its reflectance. In the four approaches below, which were considered at length, the first three consisted of ways to protect a reflective aluminium layer and the fourth explored the possibility of using total internal reflection.

3.6.1. *Dielectric-coated aluminium*

The Optical Coating Laboratories Incorporated (OCLI) [21] have produced large amounts of coated aluminium sheet for the lighting industry. Standard 0.5 mm thick pol-

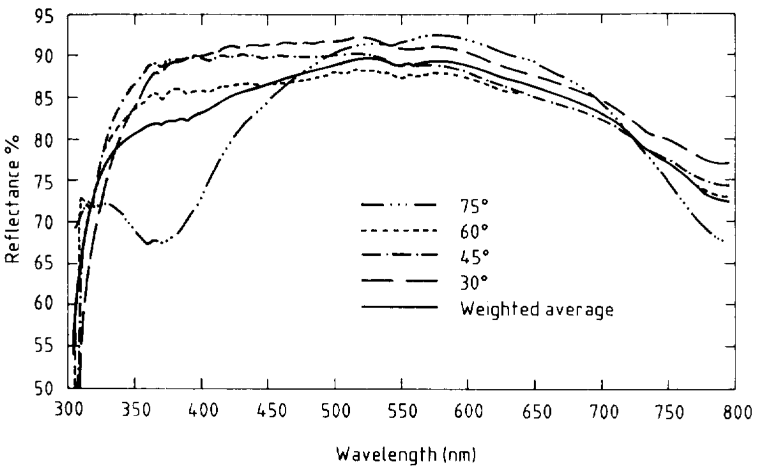

Fig. 13. Specular reflectance of dielectric-coated aluminium as a function of angle and wavelength in water. Note the loss of reflectance in the blue at large angles of incidence. The weighted average refers to the angular distribution shown in Fig. 12.

ished (on one side) anodised aluminium, with an anodised layer of 2 μm, is coated to enhance its reflectance and to protect it against weathering. This material is generally used as reflectors for strip lighting. Its reflectance in this mode is about 93% at 500 nm, which compares favourably with 82% for polished anodised aluminium alone. Early tests showed that the dielectric coating provided substantial protection against water attack. Indeed, in almost thirty years of production, the material has been shown to behave well in a great variety of weathering conditions [22].

The anodised aluminium is merely a convenient substrate and on top of this is evaporated by electron gun bombardment a thin layer of SiO_2 and a reflective layer of Al. These are followed by a low refractive index layer of MgF_2 ($n \approx 1.4$) and a high refractive index and sealant layer of a TiO_2/Pr_2O_3 mix ($n \approx 2.0$). The reflectance of the coated aluminium is optimized for an angle of incidence of 45° in air. This gives a peak of 93% at 500 nm due to constructive interference from the dielectric stack. In the red the reflectance drops to about 90% and in the near UV there is destructive interference and absorption causing the reflectance to fall from 90% at 400 nm to below 70% for wavelengths below ~ 335 nm.

In water the performance of the material [19] is very similar (see Fig. 13) with the fall-off in the near UV moved to lower wavelengths by about 15 nm i.e. the reflectance is less than 70% for wavelengths below ~ 320 nm. This performance makes the material suitable for SNO considering the range of wavelengths and angles of incidence expected operationally (see Figs. 11 and 12).

Although the standard coated aluminium is quite thin, any contaminants in the Al which are radioactive α emitters will give rise to the $^{27}Al(\alpha, p\gamma)^{30}Si$ reaction, which has a significant cross-section for the production of 6.5–7.5 MeV γ-rays (~30 mb [23]). These γ-rays will contribute to the background, and for these to be insignificant requires the aluminium to have less than 100 ppb thorium by weight (and less than 1000 ppb uranium by weight). Radioactive assays indicated that this level of purity was routinely achieved. Measurements [24] also showed that there was no significant leaching of the coated aluminium.

Because of the complexity of the multi-layer coatings and the tight tolerances on the layer thicknesses, it is not possible to produce this material on anything other than flat substrates. The multi-layer coating plant at OCLI is the largest in the world and could produce the necessary amount of coated aluminium for SNO in about a week of running. To coat inside a concentrator would require a purpose-built and costly device which could not handle more than a few concentrators at a time. For this reason the prototype coated aluminium concentrator was a polygonal approximation to an ideally shaped concentrator with curved strips of coated aluminium held in position by a plastic holder.

3.6.2. Anodised aluminium

The automotive industry has developed ways of anodising aluminium so as to give a bright corrosion-resistant surface to rival chromium plate. The thick anodised layer is treated by boiling to seal off the absorbant columnar structure of the oxide layer. Prototype concentrators were produced from spun-aluminium cones by Harjohn Ltd. [25], and then given the sealing treatment. The reflectance of the layer was about 78% at 380 nm in water at an angle of incidence of 60° [26]. However, this was partly offset by the fact that concentrators were very cheap ($C30), self-supporting, and easy to produce. Unfortunately, aging tests in hot deionized water for the equivalent of a few years at 8°C produced a thin white layer on the anodised layer. This phenomenon is known in the aluminium industry as "smutting", and the white deposit is aluminium hydroxide. It caused the reflectance to become diffuse, and the cones to be ineffective as concentrators. For this reason the material was rejected.

3.6.3. *Aluminium back-coated on glass*

An alternative to front-surface protection was to coat the aluminium on the back of a pressed or blown glass bowl of appropriate shape. This would form a mirror and a wide range of possible protective materials would be possible as there would be no optical constraints. The bowls would thus be self-supporting.

The first difficulty to be overcome was the radioactivity of the glass. Normal glass has traces of thorium, uranium, radioactive daughters, at the level of 1ppm, and this would have been intolerable for 9500 concentrators made of glass of sufficient thickness to be self-supporting (i.e. a few mm). The threshold of the detector would have been raised by a few 100 keV. For a 1 kg concentrator a limit was set at 100 ppb each of Th and U by weight. Glass for the PMT bulbs had already been identified with radioactivity levels a factor of about four less than this [27], so the problem was considered solvable.

Prototype blown-glass bowls were provided by GB Glass Ltd. [28]. The bowls were coated on the outside with aluminium and a protective thermally evaporated coating of titanium or silicon oxide [29,30]. Extensive tests using films of Al evaporated on flat glass plates had established that the coating angles needed to be within about 30° of the normal to the surface, otherwise an uneven coating resulted from shadowing effects, and this proved vulnerable to water attack [13]. These tests had also shown that the coating needed to be sufficiently thick and about 0.5 μm was found to give good protection. Because of the curvature of the bowls not all of the area could be coated in such a way easily. At the extremities of the bowl the maximum angle of deposition was greater than the critical angle for achieving water protection and the Al disappeared completely after five days immersion at 95°C. A further protective coating was therefore necessary which would also have the benefit of protecting the evaporated films of Al/TiO or Al/SiO. (Although possible to achieve satisfactory deposition over the whole bowl it would have been expensive.)

Thin (10–200 μm) paint-like coatings can be applied easily either by spraying or by dipping. Potential coatings were tested on 50 mm square samples of evaporated Al on glass. Most of these coatings failed to provide any substantial water protection to the Al film which still disappeared completely within the first 24 hr of immersion at 95°C. The list of such failures included epoxy, polyurethane and acrylic paint all of which were recommended for their water resistance. This result is not surprising, though, given the fact that all plastics are known to be permeable to water at a level which is significant over a timescale of years. Bitumastic (tar-loaded) epoxy fared slightly better in that the Al film was still present after four days immersion at 95°C, although its reflectance had deteriorated ($\sim$ 50%). A thicker coating of $\sim$ 1 mm of a silicon rubber also gave 2–3 days protection at 95° before serious pitting of the Al film developed.

Only two coatings protected the Al film from 10 days immersion at 95°: an alkyd resin-based paint loaded with glass flakes to increase the path length for water diffusing through the resin [31] and a photoresist developed for the chemical etching industry which can withstand immersion in strong acids when UV polymerized, but is attacked by strong alkalis [32]. The photoresist was preferred because the alkyd resin-based coating releases organic compounds when immersed in water and takes a long time to cure completely ($\sim$3 months).

3.6.4. *Total internal reflection film (TIRF)*

The only method pursued which did not involve aluminium was one based on "total internal reflection film" (TIRF) [33,34]. This material is fabricated from thin sheets of polycarbonate plastic (n = 1.6), with 45° parallel ridges on one side. These ridges allowed the possibility of total internal reflection for light rays making a small enough angle to the line of the ridges.

This material had the advantage of excellent aging properties (with no metallic surface to dissolve) and very low levels of radioactivity in the plastic. Prototypes made with multiple layers of TIRF worked very well in air but less so in water [17], where the range of angles where total internal reflection is possible was much reduced. It proved difficult to seal air between two layers in a simple and cost effective way; the layers themselves were quite transmissive to water on the kind of timescales involved in SNO. In the final analysis, the high cost of the material (about $C100 per concentrator) and the engineering problems of sealing in an air gap caused the idea to be abandoned.

3.7. *Selection of dielectric-coated aluminium*

At the time when a decision had to be made, two reflective materials remained: the dielectric-coated aluminium and the back-coated glass. Both had achieved good results in the aging tests conducted up to that time except for those involving extreme water conditions beyond those then expected in SNO (e.g. very high salinity, extreme pH, and the presence of certain biocides). The technology of protecting the back surface of the glass was not as well-tested as that of the dielectric-coated aluminium, but it looked like similar protection could be achieved. However, this lack of maturity in comparison to the dielectric-coated aluminium (which was a commercial product with a long history) was considered a drawback.

The mounting of the concentrator and PMT in the hexagonal cell (Fig. 3) gave the possibility of pressure being applied to the sides of the concentrator through flexure of the hexagonal cells. In the prototype coated aluminium concentrator the strips were held in a plastic bowl and this was much more flexible and robust than the prototype glass concentrator. Furthermore, the estimated cost for a glass concentrator was 40% greater than for one made from coated aluminium. For the above reasons it was decided to make a dielectric-coated aluminium strip concentrator.

4. Dielectric-coated aluminium strip concentrator

As the coated aluminium was only available in flat sheets a polygonal approximation to an ideally shaped concentrator was used with strips of dielectric-coated aluminium held in position by a plastic holder. Besides its flexibility plastic is a very suitable material as it is easy to manufacture into the required shape and typically has very low radioactivity. The design of the concentrator involved deciding on the method of mounting the strips, choosing the number of strips per concentrator, designing the plastic holder, selecting the plastic, and optimizing the dielectric coating.

4.1. The design of the holder

Although the aluminium sheet used for the dielectric-coated aluminium is pure aluminium (99.95%), the sheets are quite springy as a result of work hardening in the rolling process. In the prototype the strips were held bent in the correct shape by lips around the top and bottom of the plastic holder. This had the advantage that the strips had only to be cut out into flat strips of the appropriate shape, but it required considerable accuracy in making the holder. This is because a change in distance between the top and bottom lips directly affects the curvature of the strip and an accuracy of ~0.1 mm was required on this dimension. This is difficult as the plastic is under stress from holding the strips and also from inbuilt stresses arising in the moulding of the holders (although the latter can be relieved by annealing). These stresses give rise to creep which is considerably worse when the plastic is under water [35]: for ABS plastic the Young modulus is estimated to change by a factor of about 10 over a period of 10 years in water. Although reinforcing a plastic (e.g. by adding glass fibres) generally gives much better creep characteristics, the requirements of low radioactivity and low cost precluded this consideration.

For this reason it was decided to prebend the strips to the correct shape before assembly in the plastic bowl. This has the advantage of reducing the precision required in the manufacture of the plastic holders and of removing uncertainties over the creep of plastic during 10 years in water; however, it requires making a tool to bend every one of the strips required for the 9500 concentrators.

Prebending the strips results in stresses within the aluminium up to a maximum of about 0.4 of the yield stress i.e. about 30 N/mm^2. The effect of creep of aluminium on the curvature of prebent strips over a period of 4.5 months was measured; the bend was found to have remained the same within ±0.2 mm. Accelerated tests on prebent strips held at elevated temperatures also indicated that the effect of creep of aluminium on the curvature of the strips would be small. The retaining spigots for the dielectric-coated aluminium strips (see Section 6 below) ensured that the curvature of the strips could not increase and the tolerances were such that the curvature could only reduce by an amount which would give rise to give a maximum gap of about 2 mm between the back of the strips and the holder some 50 mm from the face of the PMT. As discussed above in Section 3.4, the effect on optical performance of such a change in shape of the concentrator would be small.

The decision on how many strips per concentrator was a compromise between the quality of angular response, which favoured a large number, and manufacturing ease which favoured a low number. In the prototype there were 24 strips per concentrator. This was reduced to 18 for the final design as the smaller number still gives a good approximation to the ideal shape (as shown in the table in Section 3.2 above), and also gives a significant saving in manufacturing cost, assembly time, and light loss between the strips (the gap between the strips was ~0.2 mm).

The design of the holder is shown in Fig. 14. The plastic holder consists of a circular bowl with an attachable rim. There are locating webs and retaining spigots for the strips and on the outside of the bowl are six bosses for holding the concentrator in its hexagonal cell. These bosses have moulded-in holes for the retaining bolts and slots for their

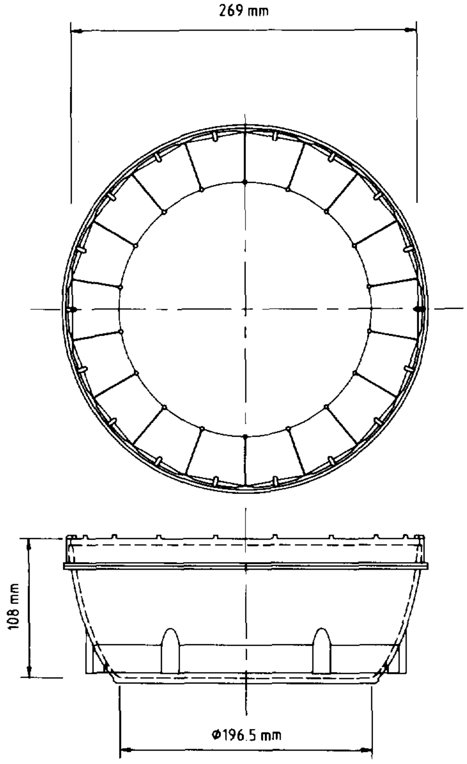

Fig. 14. Design of the concentrator. The plan view shows the retaining spigots for the dielectric-coated aluminium strips; the side view shows the bosses for holding the concentrator in its hexagonal cell and the fail-safe ledge at the join of the rim to the bowl.

nuts; moulded-in studs were not used because of the possibility of high internal stresses arising. The assembled concentrator has a ledge at the join of the rim to the bowl which provides a failsafe means of ensuring the concentrator can not come out of its hexagonal cell and fall onto the acrylic vessel. There are six small holes in the plastic bowl to reduce any gas bubbles forming when the detector is being filled with water.

For ease of manufacturing, a plastic that can be injection-moulded is required. Black ABS had already been chosen for the PMT support structure (PSUP) because it was much cheaper than any other suitable plastic, had very low radioactivity [36], no significant mass leaching [36], and a low tendency to promote biological growth [37]. Black was chosen as a colour to reduce reflections within the detector. Although its creep under stress while immersed is considerable it had been determined to be satisfactory for the stresses expected in the PMT support structure [35]. As the dielectric-coated aluminium strips are bent to the right shape the holder is under very little stress so any creep is very small. For these reasons the same type of ABS was used for the concentrators as for the support structure.

There is a further constraint on concentrator design which results from the desired water flow patterns. Ultra-pure water is injected into the detector close to the acrylic vessel as this is the region viewed by the PMTs and where purity is most important. It is desirable to achieve a light water flow pattern through the PMT and concentrator sphere (see Fig. 1) which is everywhere radially outward to avoid the risk of contaminating the water close to the acrylic vessel with water from outside this sphere, which is likely to be less pure because of the many more components which are in this region. The close fit of the top rim of the concentrator within the hexagonal cell is designed to ensure a suitably high water impedance to obtain an overpressure within the support structure sphere (Fig. 1) large enough to prevent turbulent mixing of water from the outside.

4.2. Optimization of the dielectric-coated aluminium

To check how well the optical reflectance of the dielectric-coated aluminium was matched to SNO requirements, distributions of detectable photons in terms of wavelength and angle of reflection from the concentrator were calculated from simulations. These distributions depended on the initial spectrum of Cherenkov light, the absorption of water and acrylic, the response of the PMTs [16] and the geometry of SNO. Because of the symmetry of the detector, it was not necessary to consider polarization of the Cherenkov light.

The optical behaviour of dielectric-coated aluminium was then modelled using approximate thicknesses and refractive indices of the thin film layers [19]. It was determined that the normal production dielectric-coated aluminium was fairly well optimized to SNO's requirements and that a change of more than 50% in the thickness of the films would probably be detrimental to the response of the concentrator.

Samples of dielectric-coated aluminium were made by OCLI with different coating thicknesses, up to 10% thicker and 50% thinner than normal production. The reflectance of the samples was measured [19] as a function of wavelength and angle and Fig. 15 illustrates the effect of varying the coating thickness for a 60° incidence angle in water. The two transparent layers were varied in unison as this was simple to achieve and the samples were age-tested for 10 days in 95°C water to confirm that varying the thickness of the coatings did not compromise the durability of the material.

The measured reflectances of the samples were integrated over the theoretical distributions of angle and wavelength. A merit factor was calculated for each [19], based on the efficiency for detecting photons, and a choice was made, which was 10% thinner than nominal. This caused the fall-off in the near UV to move to lower wavelengths by about 10 nm i.e. the reflectance is less than 70% for wavelengths below ~310 nm. From these measurements it was possible to calculate the mean reflectance for the dielectric-coated aluminium in operating conditions; a value of 83 ± 2% was obtained.

The following optical specifications were given to OCLI:

- The total photopic reflectance in air, i.e. specular plus diffuse reflectance weighted over the spectral sensitivity of the human eye, should be greater than 93%. This was to be measured on the Diano TR-2 reflectometer at OCLI.
- To control the coating thickness the specular reflectance in air near normal incidence was to be i) greater than 80% at 380 nm and ii) greater than 84% at 700 nm. Requirement i) ensured the coatings were thinner than 110% of optimum; requirement ii) ensured the coatings were thicker than 90% of optimum. The measurements were to be made on a Lambda-9 spectrophotometer, with a "VW" reflectometer, at OCLI.

4.3. Aging specifications and tests

The aging specification was that the dielectric-coated aluminium should be immersed in deionized water, at temperatures between 92°C and 96°C, for 10 days. At the end of this period, the total reflectance in air at near normal incidence at 500 nm should not have been reduced by more than 2%. Both sides of the anodised aluminium were coated (see below) and this test applied to both surfaces; for the front it was performed with a spectrophotometer (and visually - see below), while for the back an integrating sphere was used, because of the diffuse nature of the reflection [38].

The dielectric-coated aluminium was produced in three batches. The aging tests showed that the presence of dissolved air in the deionized water increased the attack on certain samples of dielectric-coated aluminium. With the dissolved air removed, as it will be in SNO, and the water kept under nitrogen, the coated aluminium was much more robust and survived immersion for 10 days at 95°C [39]; this work also provided evidence, from aging samples of coated aluminium at a variety of temperatures and under different

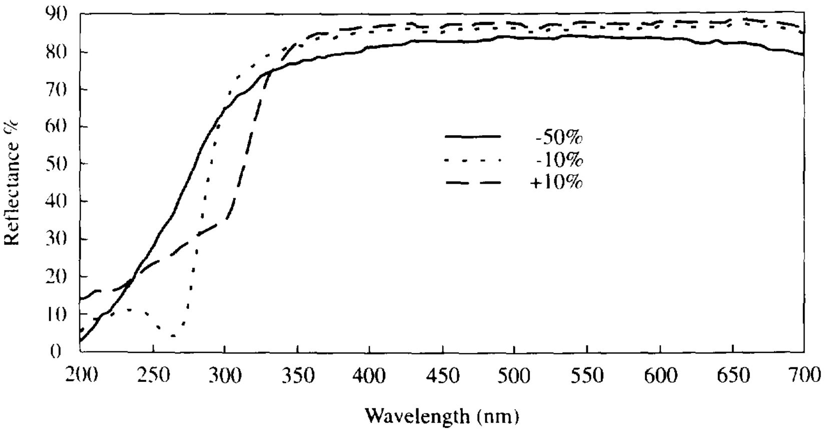

Fig. 15. The effect of dielectric-coated aluminium coating thickness on reflectance as a function of wavelength. Note that greater thicknesses increase the cut-off wavelength and vice versa.

conditions, that reaction rates increased by a factor of 2.2(2) for every 10°C rise in temperature. The aging specification was altered to include the requirement of degassing the water.

A quick and very sensitive visual test was possible because of the dip in reflectance of the dielectric-coated aluminium in the blue at grazing incidence. Fig. 13 shows this effect in water and it is much more extreme in air. The material appeared yellow when viewed close to edge-on. The lack of this yellow appearance was a definite indication of the failure of the coating and the effect on the reflectance when the coating fails is shown in Fig. 16.

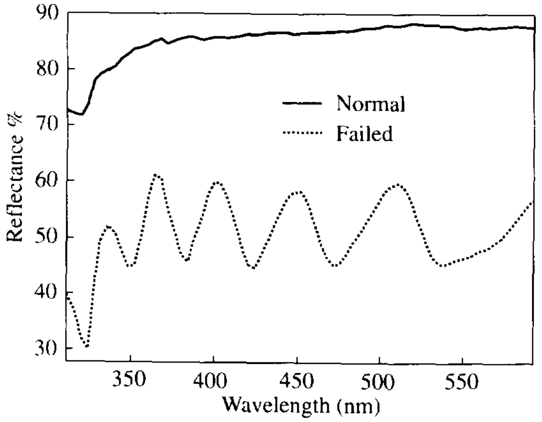

Fig. 16. An illustration of the effect on the reflectance for light incident at 60° in water when the dielectric-coating failed an aging test. The deionized water contained dissolved CO_2 and air and the reflective aluminium layer oxidized. This made the whole dielectric stack transparent, giving a response curve with ripples very similar to that of thick anodised aluminium. The loss of reflectance when the coating failed was associated with an increase in the amount of diffuse reflection. (The spectrophotometer had an acceptance angle of 2°).

4.4. Production tests

The production dielectric-coated aluminium was subjected to the standard mechanical and vapour tests which OCLI employ for their thin-film coatings. The automated rubbing test with a piece of lint demonstrated resistance to scratching. The tape test consisted of applying adhesive tape to the coating and pulling it off sharply; if some of the coating came away it appeared as a piece of reflective aluminium on the tape. This latter test was very useful in rejecting dielectric-coated aluminium which had not been properly cleaned or had been handled with bare hands before coating; this was only a very small fraction of the production.

In the course of producing the dielectric-coated aluminium it was found that there was poor water protection or adhesion of the dielectric coatings with certain rolls of anodised aluminium under certain operating conditions. As a result, in addition to the standard OCLI checks, pre-production tests on a few sheets from the selected anodised roll together with a simple on-line aging test were introduced. The aging test involved immersing the dielectric-coated aluminium in a one molar solution of NaOH for ten minutes and checking that its reflectance was not significantly affected; while not as accurate as the 10 day test in 94°C water it was introduced so that coated aluminium with poor water protection could be identified quickly and a production run halted, if necessary.

4.4.1. Protecting the back surface and edges of the dielectric-coated aluminium

Due to the regular observation of smutting on the unpolished back side of the dielectric-coated aluminium after aging in water, it was decided to coat the back side of the material. All that was needed was a layer of titanium oxide to seal against the water, but from a manufacturing point of view it was easiest to coat in an identical manner to the front. Generally the dielectric coating on the surface proved less resistant to attack by water, probably due to the anodised layer being unpolished, but was sufficiently good to eliminate the smutting.

To reduce any possibility of corrosion from the cut edges of the dielectric-coated aluminium, these were protected with titanium oxide. This was done as a separate coating, once the dielectric-coated aluminium was cut into pieces. The pieces were stacked in groups of 300 and the exposed edges were coated by thermal evaporation by Omitec Limited [30] (see Section 5.1).

4.4.2. Substrate thickness and selection of the rolls

To reduce the possibility of significant radioactive contamination, and to make the bending easier, the thickness of the aluminium substrate was reduced from the standard 0.5 to 0.3 mm. This thinner material was available in the same quality as the 0.5 mm, and was as thin as it was possible to go without encountering severe problems with the flexibility of the sheets.

In view of the possible variations in radioactive contamination of aluminium owing to differing origins and degrees of recycling, the radioactivity of the aluminium rolls to be coated was measured. Samples from candidate rolls were assayed by direct gamma counting with a germanium well detector situated in the low-background laboratory of Birkbeck College, London. All were found to have acceptable levels of radioactive contamination.

Sheets from the selected rolls were also test coated by OCLI to check for good adhesion and some were also viewed with a low voltage electron microscope to check that the dielectric coating or the anodised substrate did not appear porous.

The rolls which were selected had typically the following levels of thorium, uranium and potassium by weight [40]:

- ^{228}Ac: 33 ± 13 ppb ^{232}Th equivalent.
- ^{226}Ra: 36 ± 3 ppb ^{232}Th equivalent.
- ^{238}U: 351 ± 35 ppb.
- ^{226}Ra: 36 ± 3 ppb ^{238}U equivalent.
- ^{40}K: 0.3 ± 0.8 ppb

Simulations, using levels of 100 ppb by weight thorium and 1000 ppb by weight uranium, with the activities assumed at the bottom of the chains (where the high energy gamma-rays occur), indicated a satisfactory background level. The decay chains were out of equilibrium which is probably due to the removal of radium in the aluminium smelting process [40].

5. Concentrator production

The injection-moulded ABS plastic holders were made by Algram Limited [41] and delivered in plastic bags to reduce dust-related radioactivity problems to a minimum. The tolerances were ±0.25 mm for all the larger dimensions of the holder and ±0.1 mm for the smaller ones (see Fig. 14). The dielectric-coated aluminium was manufactured by OCLI on selected aluminium rolls and to our specifications.

5.1. Cutting and edge-coating dielectric-coated aluminium strips

The dielectric-coated aluminium sheets arrived with a protective plastic film on the highly reflective side. The sheets were cut into rectangles slightly bigger than the desired size using a guillotine. These pieces were stacked into groups of 50 and held tightly together. These stacks were machined, two at a time, by a CNC mill. It was found that CNC machining, unlike die-stamping, which would have been quicker, gave a smoother and unpitted edge surface which could be coated easily. Moreover, it did not cause such extensive fracturing of the thin films close to the edge as die-stamping.

Prior to edge coating the strips the protective plastic film was removed and the strips were cleaned ultrasonically in alcohol to remove cutting fluid, and were reassembled into stacks. These stacks were sent to Omitec for edge-coating with titanium oxide. The specification was that the thickness should be 500 nm and that the coating angles were within 20° of the normal. The coating visibly darkened the edge, which made for easy verification of the coating after age-testing; this coating has performed well under all water tests.

Low voltage electron microscope studies of the dielectric-coated aluminium indicated that there might be minute traces of the low tack, natural rubber based adhesive of the protective film remaining on the strips after cleaning. However, there was no significant effect on the reflectance of the coated aluminium and it was found in those areas where there might be traces of adhesive that the dielectric-coating was more robust under aging tests in water.

5.2. Bending

Bending the dielectric-coated aluminium to the right shape was not straightforward as the amount of bending depended on the speed of the bending operation, which meant that the operation had to be automated. The material retained a good deal of elasticity even after bending and so had to be bent to a tighter curvature than required so that it sprang back to the right shape upon release. Three identical pneumatic bending machines were constructed. They bent the coated aluminium around an aluminium former with a nylon roller at a precisely controllable speed. The resulting shape was accurate to ±0.2 mm and reproducible. A go/no-go gauge consisting of a 1 mm gap in an aluminium plate was used as a check. Test strips were age-tested after bending to see if the bending had any deleterious effects on the durability of the thin films. No such effect was detected on the front surface, but corrosion of the thin films was observed on the back at the point of greatest curvature, where the surface was under the greatest tension. Cracking of the films was observed under a microscope. However, the damage was limited to a narrow band of about 2 mm width around the point of maximum curvature and was not thought to be a concern as it did not adversely affect the reflectance of the front surface.

6. Assembly

A clean room was prepared for the assembly of the concentrators. Checks for dust contamination were made using wipe tests devised by the Cleanliness Group within the SNO collaboration [42].

To assemble the concentrator the prebent strips are first loaded into the bowl. Then the rim is slid onto the bowl in such an orientation that the retaining spigots on the rim initially line up close to the small gap between two adjacent strips. In this orientation the spigots are not touching the strips, which facilitates the mounting of the rim. After which the rim is rotated by about 10° so that the spigots just touch the centre of each strip. This rotation is determined by the movement of six pins on the rim in slots in a ledge on the bowl (see Fig. 14). Finally the rim is secured to the bowl by "heat-staking" the six pins. This involves melting the ends of the pins at about 185°C by means of a temperature-controlled soldering iron. Solvent welding of the rim to the bowl was not used because of the possibility of high inbuilt stresses arising.

Each finished concentrator was checked visually for mechanical integrity and in particular that all the dielectric-coated aluminium strips were bedded correctly.

7. Test results

Prototype PMT/Concentrator combinations were tested in a light-tight, water-filled drum, as shown in Fig. 17. The source of light was the Cherenkov radiation from ^{90}Sr, a pure β-emitter, deposited at the centre of a 30 mm diameter acrylic sphere [43]. The acrylic was the same UV-transmitting material used for the central vessel in SNO, so the wavelength distribution of detected light from this source was expected to be very similar to that which will be encountered operationally. The overall scale of the test rig was much smaller than that of SNO, however, so light absorption effects were not as large; it was estimated that the low wavelength light cut-off (at the 50% point) was 320 nm as opposed to an expected 340 nm in SNO and this would lower the measured mean reflectance by ~ 0.5%. The acrylic sphere was housed in a 50 mm diameter brass cylinder which was closed at the top so that light only shone downwards in a cone of half-angle 45°. Below the source was a concave spherical mirror arranged so that the PMT/concentrator was illuminated by a parallel, upward-going beam of light. The non-uniformity of the beam, including the blocking effects of the source itself, was taken into account in the analysis. The PMT/concentrator was rotated with respect to the light beam to measure an angular distribution; effects of the earth's magnetic were eliminated with a pair of Helmholtz coils outside the drum.

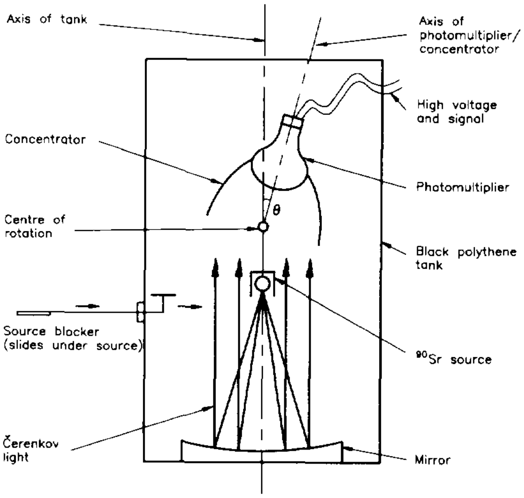

Fig. 17. Sketch of the apparatus for measuring the concentration factor and the angular response of a PMT/Concentrator in water and in air.

The photoelectron count as a function of angle is shown for a prototype glass concentrator in air in Fig. 18 and for a production dielectric-coated aluminium strip concentrator in water in Fig. 19. The rate is normalized to the rate observed in the PMT without the concentrator with the PMT axis parallel to the beam of light. A factor of $\cos\theta$ has been introduced in Fig. 18, but not in Fig. 19, to account for the change in solid angle of the concentrator aperture as θ changes.

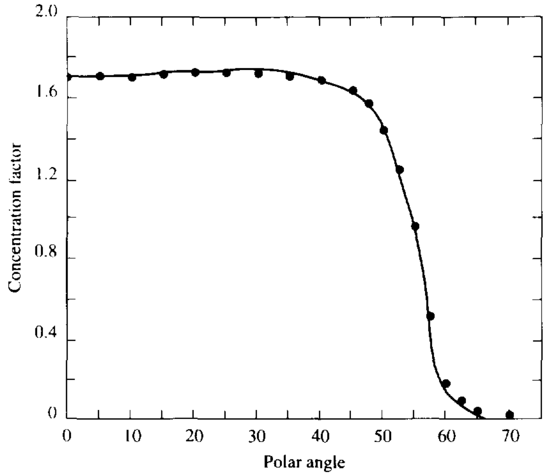

Fig. 18. Measured angular response for aluminium coated glass concentrator as a function of the polar angle in air. The points are well fitted by a simulation which assumes an aluminium reflectance of 84%. A factor of $\cos\theta$ has been introduced to account for the change in solid angle of the concentrator as θ changes.

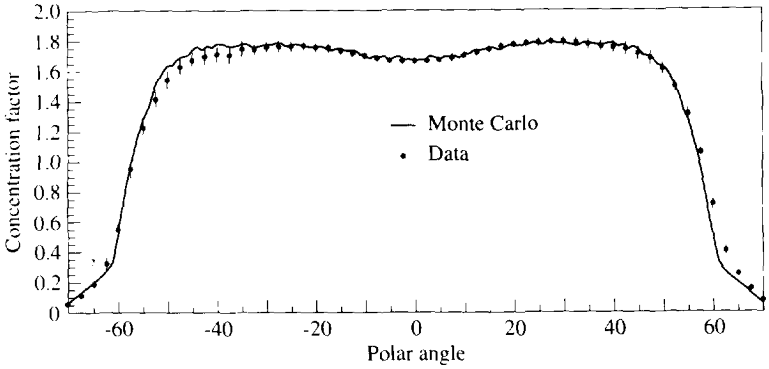

Fig. 19. Measured angular response for a production dielectric-coated aluminium strip concentrator as a function of polar angle in water [44]. The points are well fitted by a simulation [14] which assumes a mean reflectance of dielectric-coated aluminium of 82%.

The angular dependence of the concentrator factor is predicted by Monte Carlo simulations [14] to only alter by ±1.5% over the wavelength range 350 to 500 nm and the Monte Carlo curve in Fig. 19 is for 400 nm. The mean value of the reflectance of dielectric-coated aluminium in water for the wavelength distribution expected in SNO (see Fig. 11) was measured to be 82 ± 3% The result is consistent with that deduced from measurements on a single flat strip of dielectric-coated aluminium, which was 83 ± 2%.

8. Conclusion

In this work we have made a case for using light concentrators in large water Cherenkov detectors, and have demonstrated that they have the desired optical characteristics. We have enumerated all the salient points in the selection of materials, of which durability in water was the most difficult to obtain. The basic steps of manufacture and quality control have also been discussed.

Acknowledgements

A large number of personnel have been involved in this project. Many have been referenced explicitly in the text. Others include: various members of the Oxford Nuclear Physics Workshop, in particular, Keith Nobbs who did all the CNC machining, Bill Linford who designed and made the bending machines and Mick Williams for all his organisational work; Gary Smith of OCLI for all his help on the optimization of the dielectric-coated aluminium; Bernard Menzies and his team at Algram who made the plastic holders; Al Morgan and Roger Every who did the engineering drawings; Alan Holmes for his advice on the design; Ron Marsh and Robert Munday and the team at Omitec who edge-coated all the dielectric-coated aluminium strips; Alan Poon who did much early work on dielectric-coated aluminium durability; Ray Saunders and his team at Acuvac for their work on the prototype plastic holders; Andi Clements from RAPRA for advice on plastics; David Hyde and Mike Kendal of Kendal and Hyde for their work on evaporated protective films; M. Turek of UKAE for the low voltage electron microscopy; R. Bulpett, Experimental Techniques Centre, Brunel University for his valuable help in the surface analysis of various dielectric-coated aluminium samples, Walter Davidson of the NRC Canada for his work on anodised aluminium and Kevin Lesko of the LBL for discussions on the hexagonal cell mounting. We thank them all.

The authors would also thank the UK Particle Physics and Astronomy Research Council and the Canadian Natural Sciences and Engineering Research Council for the provision of funding for this project.

References

[1] J.V. Jelley, The Cherenkov Radiation and its Applications (Pergamon, New York, 1958).
[2] G.T. Ewan, Nucl. Instr. and Meth. A 314 (1992) 373.
[3] C.E. Waltham et al., Physics in Canada 48 (1992) 135.
[4] R.M. Bionta et al., Phys. Rev. Lett. 58 (1987) 1494; and C.B. Bratton et al., Phys. Rev. D 37 (1988) 3361.
[5] K.S. Hirata et al., Phys. Rev. Lett. 58 (1987) 1490; and and Phys. Rev. D 38 (1988) 448.
[6] Y. Suzuki, Proc. TAUP93, eds. C. Arpesella et al., Nucl. Phys. B (Proc.Suppl.) 35 (1994) 273.
[7] SAGE Collab., A.I. Abazov et al. Phys. Rev. Lett. 67 (1991) 3332; and V.N. Gavrin et al., Proc. TAUP93, eds. C. Arpesella et al., Nucl. Phys. B (Proc. Suppl.) 35 (1994) 412.
[8] GALLEX Collab., P. Anselmann et al. Phys. Lett. B327 (1994) 377.
[9] J. Bahcall, Neutrino Astrophysics (Cambridge, 1989); and S. Tuck-Chièze et al., Phys. Rep. 230 (1993) 57.
[10] S.P. Mikheyev and A.Y. Smirnov, Nuovo Cimento 9C (1986) 17; and L. Wolfenstein, Phys. Rev. D 20 (1979) 2634.
[11] W.T. Welford and R. Winston,Optics of Nonimaging Concentrators: Light and Solar Energy (Academic Press, 1978); W.T. Welford and R. Winston, High Collection Nonimaging Optics (Academic Press, 1990); and R. Winston, Nonimaging Optics, Sci. Amer. 264 (1991) pp.76-81.
[12] M.E. Moorhead and N.W. Tanner, Light reflecting concentrators for photomultipliers with curved photocathodes, Oxford University Preprint OUNP-95-25, submitted to Appl. Optics.
[13] M.E. Moorhead, D. Phil. thesis, Oxford University, unpublished (1992).
[14] M.D. Lay, D. Phil. thesis, Oxford University, unpublished (1994).

[15] T.J. Radcliffe and J.R. Leslie, private communication, 1991.
[16] M.E. Moorhead and N.W. Tanner, Optical Properties of the K-Cs Bialkali Photocathode, Oxford University Preprint OUNP-91-05, submitted to Nucl. Instr. and Meth.
[17] G. Ouellette, C.E. Waltham, R. Meijer Drees, A. Poon, R. Schubank, and L.A. Whitehead, Appl. Opt. 31 (1992) 2360.
[18] M. Lowry, private communication, 1991.
[19] S. Gil, G.A. Clarke, L. McGarry and C.E. Waltham, Appl. Opt. 34 (1995) 695.
[20] C.E. Waltham, J. Boyle, W. Ramey and J. Smit, Appl. Opt. 33 (1994) 7536.
[21] Optical Coating Laboratories Inc., Santa Rosa CA 95407-7397, USA.
[22] G. Smith, OCLI, private communication, 1992.
[23] G. Dearnaley et al., Phys. Rev. 139 (1965) B1170.
[24] X. Zhu, B. Sur, H. Lee and A.B. McDonald, SNO Scientific and Technical Report, SNO-STR-91-065..
[25] Harjohn Industries Ltd., 128 Grantham, St. Catharines, Ontario L2P 3H2, Canada.
[26] W.F. Davidson, NRC Ottawa, private communication, 1989.
[27] Schott Glaswerke, Hattenbergstrasse 10, D-6500, Mainz 1, Germany.
[28] GB Glass Ltd., Lemington, Newcastle upon Tyne NE15 8SX, UK.
[29] Kendall Hyde Ltd., Kingsland Industrial Park, Stroudley Rd., Basingstoke, Hants RG24 8UG, UK.
[30] Omitec Electro-Optics Ltd., Wills Road, Industrial Estate, Totnes, Devon TQ9 5XR, UK.
[31] Finnigan's Smoothrite, Hunting Specialised Products (UK) Ltd., Eltringham Works, Prudhoe, Northumberland NE42 6LP, UK.
[32] Supplied by Alpha Metals, 1 The Broadway, Tolworth, Surbiton, Surrey KT6 7DQ, UK.
[33] Available from TIR Systems Ltd., 3935 2nd Ave., Burnaby B.C., Canada V5C 3W9.
[34] L.A. Whitehead, R.A. Nodwell and F.L. Curzon, Appl. Opt. 21 (1982) 2755.
[35] H. Leung, SNO Scientific and Technical Report, SNO-STR-92-055 (1992).
[36] P.T. Trent, SNO Scientific and Technical Report, SNO-STR-92-006 (1992).
[37] J. Smit and W. Ramey, private communication, 1992.
[38] L. McGarry, M.Sc. thesis, University of British Columbia, unpublished (1992).
[39] R. Newman, SNO Scientific and Technical Report, SNO-STR-95-035 (1995).
[40] J.C. Barton, Nucl. Instr. and Meth. A 354 (1995) 530.
[41] Algram Engineering Company Ltd., Eastern Wood Road, Langage Industrial Estate, Plympton, Plymouth PL7 5ET, UK.
[42] R. Stokstad, private communication, 1993.
[43] R.J. Boardman, M.D. Lay, N.W. Tanner and D.L. Wark, Nucl. Instr. and Meth. A 345 (1994) 356.
[44] M.J. Lyon, first year graduate research report, unpublished (1994).